MAGNETICALLY CLOSED REGIONS IN THE SOLAR WIND

A. GERANIOS*

Max-Planck-Institut für Aeronomie, D-3411 Katlenburg-Lindau, F.R.G.

(Received 6 April, 1981)

Abstract. Interplanetary plasma and magnetic field data collected by Helios-1, Helios-2 and IMP-8 satellites over the periods December 1974–December 1976, January 1976–December 1976 and December 1974–December 1976, respectively, are analysed. From this analysis, we identified 85 about cases in which the proton temperature was very low. In 50 of these cases, the interplanetary magnetic field showed characteristic variations favorable for closed structures in the solar wind.

By using the calculated radial temperature gradients as a function of the solar wind speed and the heliocentric distance we were able to identify 'cold' protons in the neighborhood of the Sun (0.3 AU).

The estimation of the distance at which regions of cold protons are formed (10 $R_\odot$) shows that this distance is the same whether we are using solar wind plasma data measured in fixed or in varied heliocentric distances.

1. Introduction

Since 1973, when observations and analysis of the Very Low Temperatures (VLT) in the solar wind have started (Gosling *et al.*, 1973), there is not a unique interpretation for this phenomenon up to day. The majority of the related papers, based on hourly or 3-hourly solar wind temperature data at 1 AU, suggest the closed Interplanetary Magnetic Field (IMF) configuration as a possible cause of such low temperatures, i.e., lower than 0.5×10^5 K for electrons and 1.5×10^4 K for protons at 1 AU (Feldman *et al.*, 1973; Gosling and Roelof, 1974; Montgomery *et al.*, 1974; Krimigis *et al.*, 1976). Under certain conditions, a contradiction to this model appeared in a paper by Geranios (1978).

Due to the fact that such low temperatures appear not only after interplanetary shock waves (which favorate the closed model, Montgomery *et al.*, 1974), but predominantly during the fall-off of solar wind streams, an attempt is made to relate these cool regions with the 'deceleration' of the solar wind which takes place in the decreasing speed-phase of a stream (Geranios, 1980; Geranios, 1981).

Analysis of solar wind plasma data from Helios-1 and Helios-2 showed for the first time cool protons in distances shorter than 1 AU. These observations coincided with IMF boundaries, regions which because of the opposite directed IMF are very appropriate to form closed magnetic field structures (Schwenn *et al.*, 1978).

The theoretical model we are treating here, assumes that the regions where VLT's occure are not magnetically connected to the Sun, and that the temperature decreases of protons are, therefore, a consequence of the lack of thermal connection with the corona.

The radial development of the proton temperature within such regions is then

* Now at the Nuclear Physics Laboratory, Cosmic Ray Group, Solonos str. 104, University of Athens.

Astrophysics and Space Science **81** (1982) 103–122. 0004–640X/82/0811–0103$03.00.

determined by an expansion (not adiabatic) as they move radially outward from the Sun.

Proton data are investigated and the temporal (and, therefore, also spatial) evolution of the inner temperature is compared with that based on experimentally derived radial temperature gradients of the ambient solar wind. The point (radial position), where the two temperatures are equal (at least on the basis of model used) must be the point where the particles 'inside' have been thermally decoupled from the corona, i.e., this point defines the origin of the 'cold region' – if such regions are indeed the major cause of VLT's.

2. Observations

Interplanetary plasma data collected over a period of about two years by solar wind plasma experiments on board the Helios-1, Helios-2, and IMP-8 satellites are used in order to identify regions, in which the solar wind proton temperature is anomalously low (Rosenbauer *et al.*, 1977; Bame *et al.*, 1976). The corresponding periods are, January 1975–Decmber 1976 for Helios-1, January 1976–December 1976 for Helios-2, and December 1974–December 1976 for IMP-8.

For the identification of a VLT in the solar wind plasma, based on 15-min averaged values, a proton temperature threshold (T_{thr}) of 1.5×10^4 K at 1 AU is required. This value is the mean proton low temperature of 30 about VLT's, analysed in the past (Geranios, 1978).

For temperature data measured in radial distances shorter than 1 AU (in the case of Helios-1, -2), and in order to define an analogous upper temperature limit, we have to take into account the increase of the temperature toward the Sun.

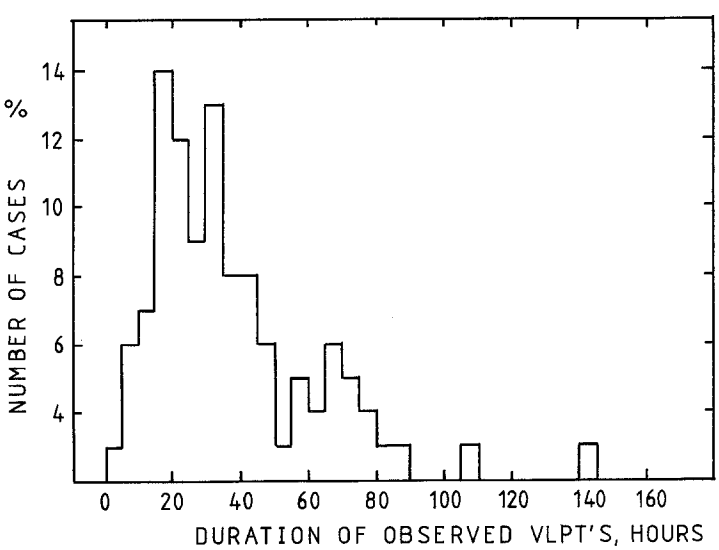

Fig. 1. The duration of the observed Very Low Proton Temperatures listed in Table I.

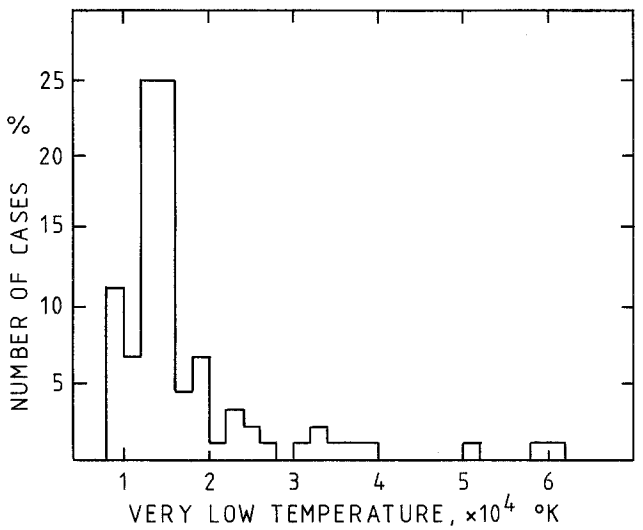

Fig. 2. The distribution of the VLT's, observed by Helios-1, Helios-2 and IMP satellites (T_m, Table I).

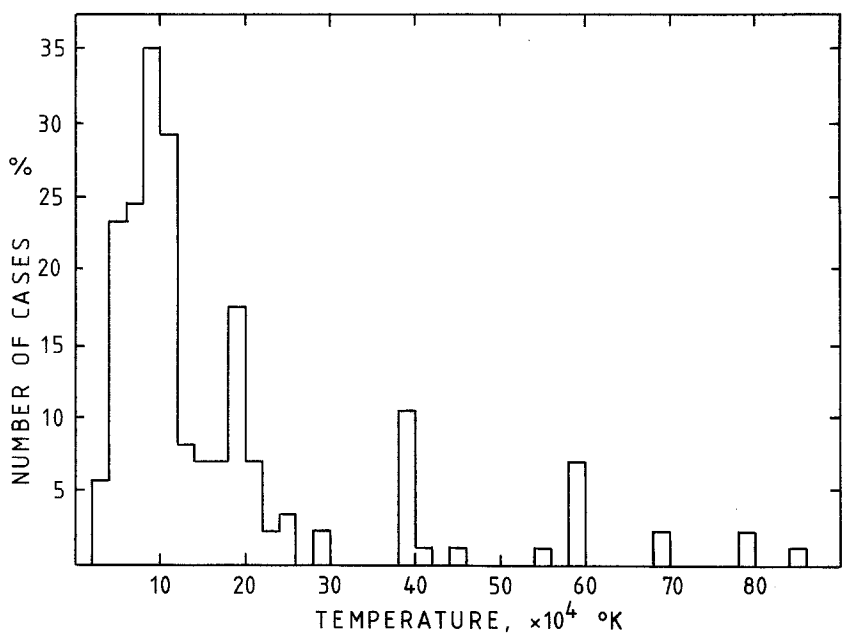

Fig. 3. The distribution of the temperatures in the ambient solar wind (T_1 and T_2, Table I).

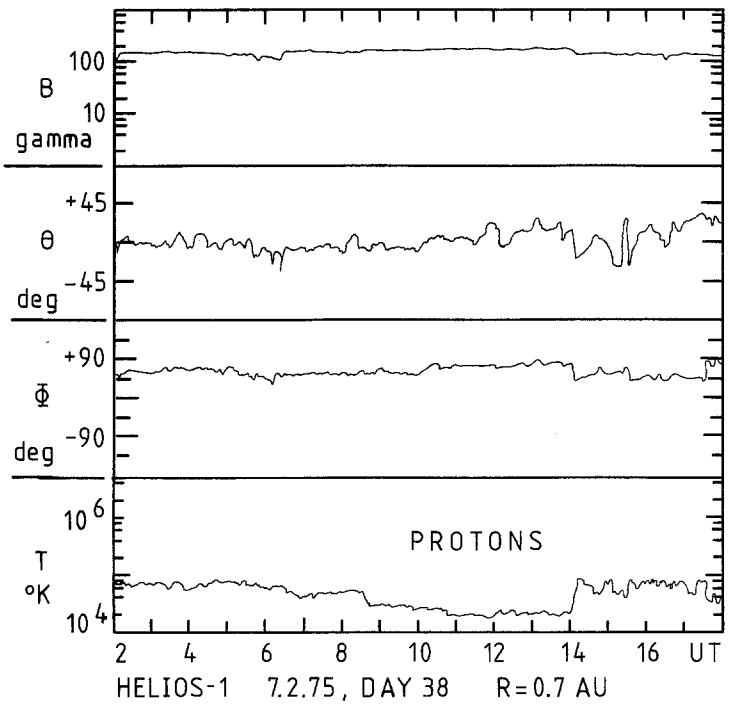

Fig. 4. A VLT region observed by Helios-1 at a heliocentric distance of 0.7 AU. B, θ, and ϕ are the interplanetary magnetic field magnitude, elevation with respect to the ecliptic plane and azimuth of the projection onto the ecliptic plane, respectively. T_r is the proton radial temperature. This VLT has a π-like feature.

On the whole, we identified 87 cases, the temperature of which was lower than the calculated temperature-thresholds.

The average duration of such cold regions is about 40 hr. (A histogram indicating this distribution is shown in Figure 1.) The mean temperature minimum inside the region (T_m) observed is about 1.8×10^4 K and the temperature outside this region is about 1.8×10^5 K, a difference of one order of magnitude. (Histograms for the distribution of these temperatures are shown in Figures 2 and 3.)

The major characteristics of the classified VLT's are shown in Table I – i.e., the onset of the decrease (day, month, and hour in UT), the duration in hours, the minimum temperature (T_m), the outside temperatures (T_1 and T_2, one before the other after the low temperature region), the corresponding minimum speed (V_m), and the simultaneous to T_1, T_2 speeds (V_1, V_2), the radial distance of the observation and the measuring spacecraft.

Except of plasma observations, for the identification of a possible VLT, the simultaneously measured IMF is also taken into account (Neubauer *et al.*, 1977) in order to distinguish any possible magnetically 'closed' structures, and therefore disconnection from the hot corona, which could cause the observed temperature depressions.

TABLE I
Characteristics of VLP temperatures

No.	Onset d/m/h UT	Duration h	T_m K ($\times 10^3$)	T_1 K ($\times 10^4$)	T_2 K ($\times 10^4$)	V_m (km s^{-1})	V_1 (km s^{-1})	V_2 (km s^{-1})	R AU	Satellite
	1975									
1	23.1:21	14	19	10	6	360	400	390	0.82	Helios-1
2	7.2:06	8	20	6	8	373	450	420	0.69	„
3	4.3:11	18	35	60	100	418	600	520	0.38	„
4	13.3:01	10	52	20	60	304	380	500	0.31	„
5	18.3:18	17	24	80	20	390	470	420	0.32	„
6	19.3:17	3	39	20	21	319	400	350	0.32	„
7	29.3:11	41	24	20	10	260	250	290	0.44	„
8	14.4:01	18	14	11	11.5	372	430	400	0.63	„
9	16.4:05	20	18	8	8.5	357	320	380	0.66	„
10	17.4:06	42	14	10	11	336	350	410	0.66	„
11	20.4:14	60	13	10	15	335	400	400	0.71	„
12	6.7:13	18	10	4	2.2	306	310	300	0.96	„
13	3.8:06	48	13	10.2	40	325	360	600	0.80	„
14	15.8:05	24	20	10.5	10	350	430	350	0.70	„
15	8.9:14	58	34	45	70	305	650	650	0.39	„
16	18.9:12	27	37	40	15	323	450	280	0.39	„
17	20.9:14	68	26	20	40	258	300	350	0.31	„
18	9.10:18	42	14	20	60	329	320	530	0.49	„
19	24.10:06	12	16	6	20	329	330	390	0.66	„
20	15.11:02	78	10	10.5	11	340	420	380	0.86	„
21	11.12:04	64	16	10	20	317	400	400	0.97	„
	1976									
22	10.1:02	16	15	11.5	40	400	430	520	0.97	„
23	27.1:12	70	17	6	20	315	330	500	0.89	„
24	12.2:18?	32?	19	20	25	360	470	520	0.78	„
25	12.3:17	32	25	11	80	331	400	610	0.46	„
26	22.3:01	68	33	22	60	374	350	310	0.34	„
27	26.3:14	28	60	60	55	340	500	500	0.32	„
28	1.4:01	72	62	40	40	306	400	620	0.32	„
29	4.5:08	50	16	20	20	334	430	380	0.70	„
30	14.5:10	72	15	15	8	327	500	300	0.80	„
31	31.5:02	84	12	30	20	319	500	600	0.92	„
32	4.6:14	145	10	20	21	304	580	620	0.93	„
33	2.7:12	88	13	10	40	315	400	600	0.99	„
34	18.10:22	32	23	20	20	310	370	400	0.43	„
35	30.10:22	27	16	10	10	305	310	320	0.58	„
36	1.11:00	60	20	10	10.5	295	320	300	0.60	„
37	3.11:14	44	16	10.5	9.5	293	300	330	0.63	„
38	18.11:00	32	18	10	9	334	400	330	0.77	„
39	22.11:19	17	12	10	6	326	350	350	0.81	„
40	30.11:10	34	13	7	20	318	370	400	0.86	„
41	25.12:12	108	12	9.5	25	358	400	450	0.97	„
42	23.2:06	24	15	4	6	323	370	330	0.85	Helios-2
43	28.2:01	14	15	12	20	530	600	500	0.82	„
44	13.3:02	34	17	20	70	384	410	620	0.68	„
45	21.3:23	36	19	10	10	301	400	310	0.58	„
46	3.5:10	34	27	20	10	316	420	310	0.46	„
47	14.11:04	8	32	20	25	348	400	390	0.58	„

Table I (*continued*)

No.	Onset d/m/h UT	Duration *h*	T_m K ($\times 10^3$)	T_1 K ($\times 10^4$)	T_2 K ($\times 10^4$)	V_m (km s^{-1})	V_1 (km s^{-1})	V_2 (km s^{-1})	R AU	Satellite
48	22.11:18	38	22	10	10	345	370	310	0.69	„
49	26.11:05	24	16	20	6	295	400	280	0.72	„
50	27.11:07	20	13	6	8	297	290	300	0.73	„
51	14.12:08	22	14	12	6	336	400	300	0.87	„
52	20.12:10	43	15	7	8	372	420	320	0.91	„
53	26.12:20	56	15	8	12	326	350	420	0.94	„
54	29.12:06	21	14	12	4.2	403	470	400	0.95	„
	1974									
55	29.12:08	25	15	15	6	420	460	400	1.0	IMP-8
	1975									
56	1.1:01	72	11	20	40	310	500	500	1.0	„
57	8.1:05	52	15	60	23	550	730	600	1.0	„
58	25.1:07	48	14	4.2	14	320	350	380	1.0	„
59	8.2:15	6	15	11	10	400	420	380	1.0	„
60	8.3:06	24	14	6	7	370	400	330	1.0	„
61	22.3:02	20	10	4.2	10	330	330	330	1.0	„
62	23.3:17	15	15	11	10	360	400	400	1.0	„
63	19.4:22	18	14	7	10	300	340	360	„	„
64	15.5:12	27	11	6	40	300	320	520	„	„
65	25.5:14	16	14	10	11	420	430	430	„	„
66	24.6:04	35	14	42	85	310	330	350	„	„
67	4.7:00	76	14	15	14	350	450	350	„	„
68	8.8:13	15	15	10	9	370	420	400	„	„
69	9.8:07	21	15	10	11	370	410	400	„	„
70	5.9:00	35	10	4.2	16	300	300	370	„	„
71	15.9:14	46	15	10	20	380	460	530	„	„
72	29.9:23	29	10	8	6.5	300	350	320	„	„
73	2.10:03	33	10	4	4.1	260	280	300	„	„
74	23.10:08	14	14	4	6	310	330	320	„	„
75	16.11:23	43	15	9	15	380	420	380	„	„
76	20.11:18	19	15	12	20	450	450	450	„	„
77	27.11:15	40	10	7.5	23	360	400	450	„	„
	1976									
78	23.2:18	66	13	9	7	300	430	330	„	„
79	22.3:16	32	15	10	9	320	380	400	„	„
80	24.3:12	36	10	8	6	310	380	340	„	„
81	14.6:4	40	11	10	4.5	320	400	330	„	„
82	13.7:01	65	14	10	20	300	400	500	„	„
83	18.8:09	23	14	10	12	360	380	400	„	„
84	21.10:18	26	13	6	5.5	320	350	340	„	„
85	6.11:12	30	10	10	11	305	350	310	„	„
86	20.12:13	38	15	10	11	390	400	360	„	„
87	29.12:09	22	13	10	9	400	500	400	„	„

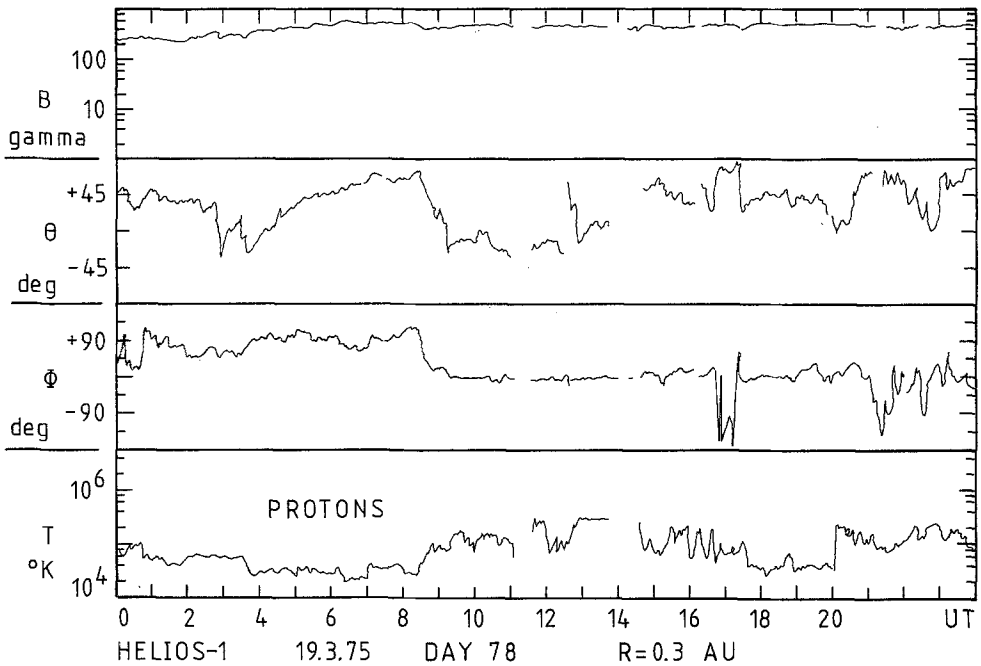

Fig. 5. A more complex example of VLT's, measured by Helios-2 near the Sun, illustrating at least two 'cool' regions. More than one π-like features of ϕ can be seen. The corresponding enhancement of B can hardly be seen because of the already high value and the logarithmic scale used.

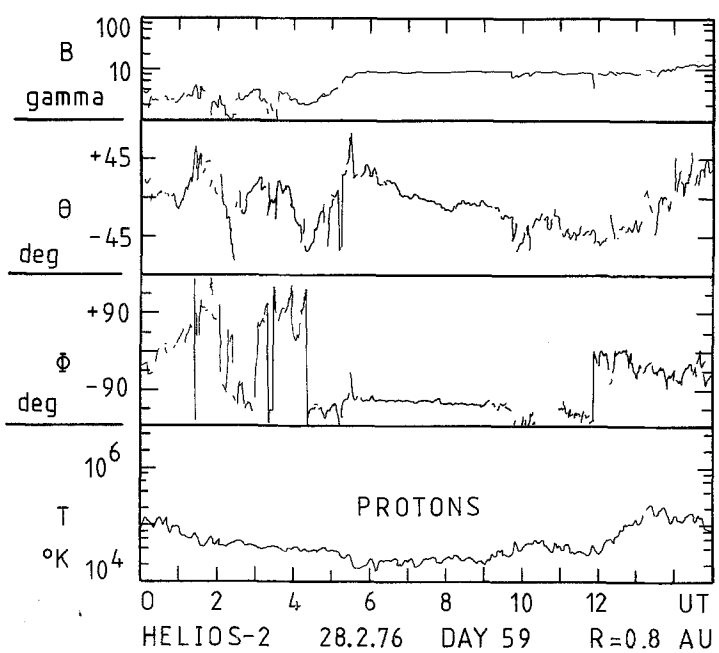

Fig. 6. An example, in which the ϕ variation displays maximum values and shows a scharp π-like feature.

Some examples for typical VLT's are briefly described.

(a) On 7 February, 1975 (Day 38) Helios-1 measured a low temperature region between ~6:30–14:00 UT with a lowest value of about 2×10^4 K, (lower panel, Figure 4). The simultaneously measured IMF magnitude B (quite intense but more or less stable) shows a π-like structure defined by the enhancement at ~6:30 UT and the decreament at ~14:00 UT. In addition, the direction of the field, ϕ projected onto the ecliptic plane, displays a similar π-like variation at almost the same times which define the duration of this structure. This variation, is of the order of 20–40°. Note that 0° indicates a direction toward the Sun and 180° indicates a direction away from the Sun. The elevation θ with respect to the ecliptic plane, displays a rather varying profile, ranging from 30 to −30°, above and below the ecliptic plane, respectively.

(b) This example (19 March, 1975, Day 78), displays at least two low temperature regions, the boundaries of which cannot be well defined (probably, ~01:00–09:00, and ~17:00–20:00 UT, Figure 5). Nevertheless, the angle ϕ shows a π-like feature, which in the first region overlaps with the low proton temperature, while in the second is a little larger. The lowest temperature value in a distance of 0.3 AU only, is 2×10^4 K. The angle θ varies by more than 90°, while B is very intense. The major difference

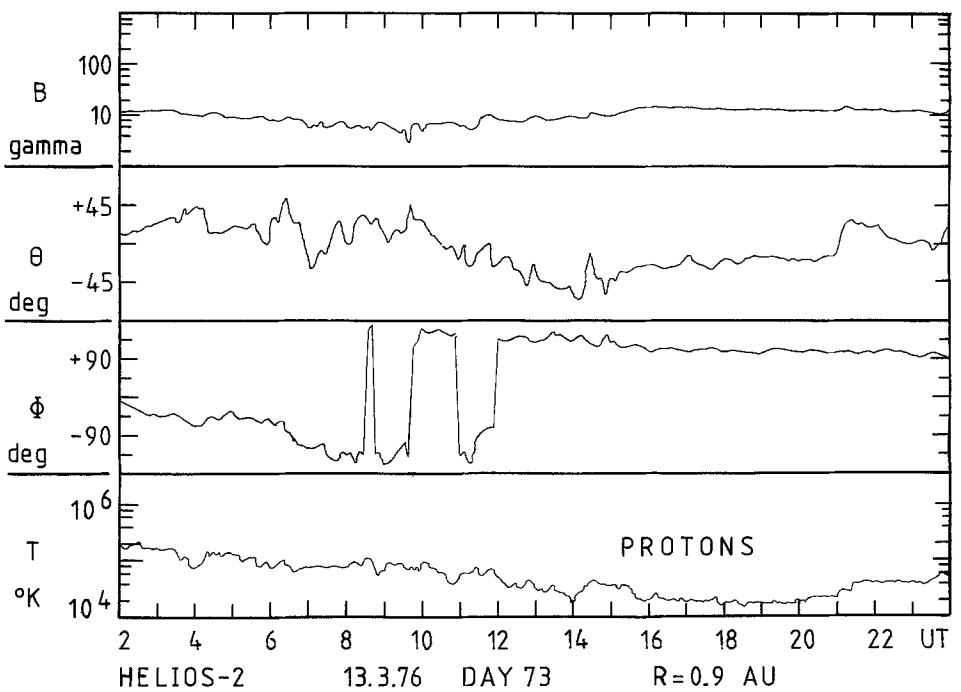

Fig. 7. This VLT is related with a magnetic sector boundary crossing, as it is shown from the angle ϕ. This observation is made by Helios-2 quite far from the Sun.

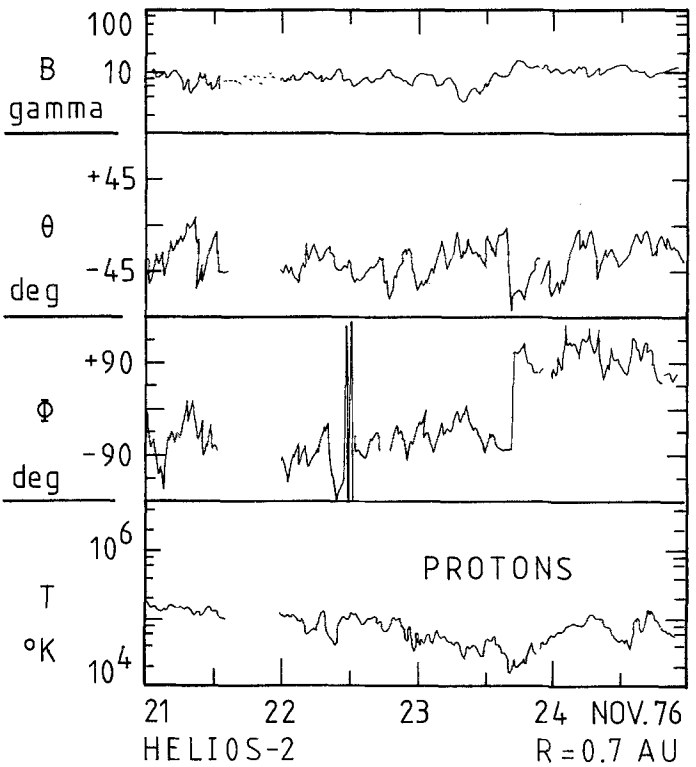

Fig. 8. This low temperature region is also related with a sector boundary from an away to a toward direction of the interplanetary magnetic field. The minimum temperature is below 2×10^4 K.

between the case depicted in the previous figure and here, is the variation of ϕ, which in this example amounts more than 100°.

(c) This third example (28 February, 1976, Day 59), has a much more pronounced variation of ϕ (pi-like again), between ~04:00 and ~12:00 UT (Figure 6). B varies also by a similar way, while θ exceeds the limits of variation of the previously mentioned examples. The proton temperature profile has no well define limits, its lowest value being less than 2×10^4 K.

(d) This low temperature region (13 March, 1976, Day 73), second half on the right of Figure 7), should be related with a magnetic sector boundary from an away to a toward direction, which is shown by ϕ. B fluctuates arround 10γ and θ changes dramatically at the boundary.

(e) The last example (23 November, 1976), presents a low temperature region which also coincides with a sector boundary from an away to a toward direction of the field. θ tends to follow a similar variation, while B does not show any peculiar behaviour (Figure 8). At least in one case, we claim that a successive observation of a cold region by Helios-2 and then by Helios-1 is made. Figure 9 shows the variation of B, θ, ϕ, V, and T for both spacecraft. Apparently, this low temperature region (having its minimum at

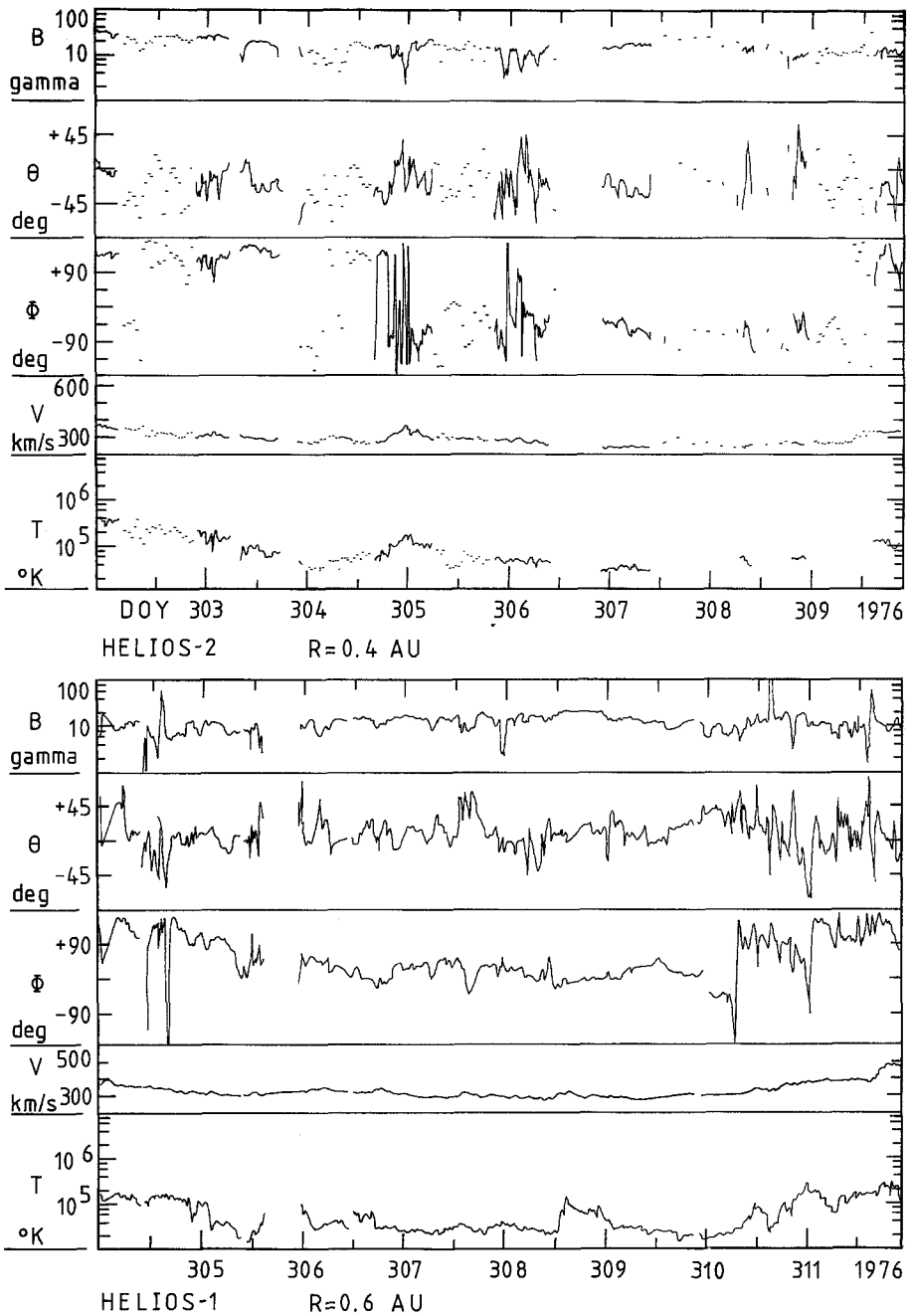

Fig. 9. A low temperature region successively seen by Helios-2 and then by Helios-1, related with a magnetic sector boundary passage. This time, the satellites were radially lined-up with a radial separation of 0.2 AU. The temperature minima (Day 304 for Helios-2, and Day 305 for Helios-1) are separated by about 30 h. The time which the structure needed to travel from Helios-2 to Helios-1, is consistent with the time calculated from the distance (0.2 AU) and the speed of propagation (300 km s^{-1}). This speed (the speed of solar wind also), is nearly constant between the two spacecraft, as it is shown by *V*.

the beginning of Day 304) correlates with a magnetic sector boundary observed by Helios-2 in the second half of the Day 304 at 0.4 AU. This region, we believe, is observed by Helios-1,30 about hours after, having its minimum temperature at midday of Day 305. This day, Helios-2 and Helios-1 were nearly radially lined-up (spacecraft-Sun-Earth angle 30° about), and the distance in between was 0.2 AU. Because the solar wind speed (V) in these days was rather constant (~ 300 km s^{-1}), we were able to estimate the time required for the assumed closed structure to propagate from Helios-2 to Helios-1, which is close to 30 hr also.

The described examples distinguish two categories of cold plasma cases. The first, is characterized by a sector boundary of the IMF and the second by a double change of the direction of the field (pi-like).

On the whole, from 85 defined VLT's (Table I), 14 show this structure and 35 are related with IMF sector boundaries.

3. Proton Temperature Gradients

The calculation of solar wind temperature gradients is one of the most important parameters for the understanding of the heat transport from the solar corona to the interplanetary space. Several theoretical models treating the solar wind as one-, two-, or multifluid involved the temperature gradients in order to predict the values of the main plasma parameters at the distance of 1 AU, which first was explored by a series of geocentric satellites (Parker, 1958; Sturrock and Hartle, 1966; Yeh, 1970; Montgomery *et al.*, 1968).

Solutions of the equation of mass, momentum and energy conservation in the solar wind assumed as one-fluid, steady, and spherically-symmetric expanding, gave temperature gradients like $-\frac{2}{7}$, $-\frac{2}{5}$, and $-\frac{4}{3}$, the last value corresponding to an adiabatic expansion, (Hundhausen, 1972). These types of solutions are studied by several authors in the past, as for example Chamberlain (1965), Parker (1964), Noble and Scarf (1963), Whang and Chang (1965), Durney (1971), and Parker (1965).

With similar treatment of the equations of mass, momentum and energy conservation but, assuming the solar wind as two-fluid (very low density in interplanetary space leads to very low collision frequencies), Sturrock and Hartle (1966) predicted temperature gradients $-\frac{2}{7}$ for electrons and $-\frac{6}{7}$ for protons. In order to elevate the solar wind proton temperature above that predicted by the basic two-fluid model, without elevating the already too high electron temperature at 1 AU. Hartle and Barnes (1970) added in the energy equations an extended heating source. In this way, they predicted different proton temperature gradients than these predicted by the basic two-fluid model. For the distance $2R_\odot$–$38R_\odot$, the gradient was about $-\frac{3}{9}$ and for the distance $38R_\odot$–$1000R_\odot$ was $-\frac{5}{4}$, ($R_\odot$ is the solar radius).

As it was mentioned in the observational part, in order to search for VLT's in distances shorter than 1 AU, because of the hotter plasma closer to the Sun, we have to calculate first the temperature radial gradients of the ambient solar wind. (Due to the availability of proton data only, we do not include electron temperature gradients.) In

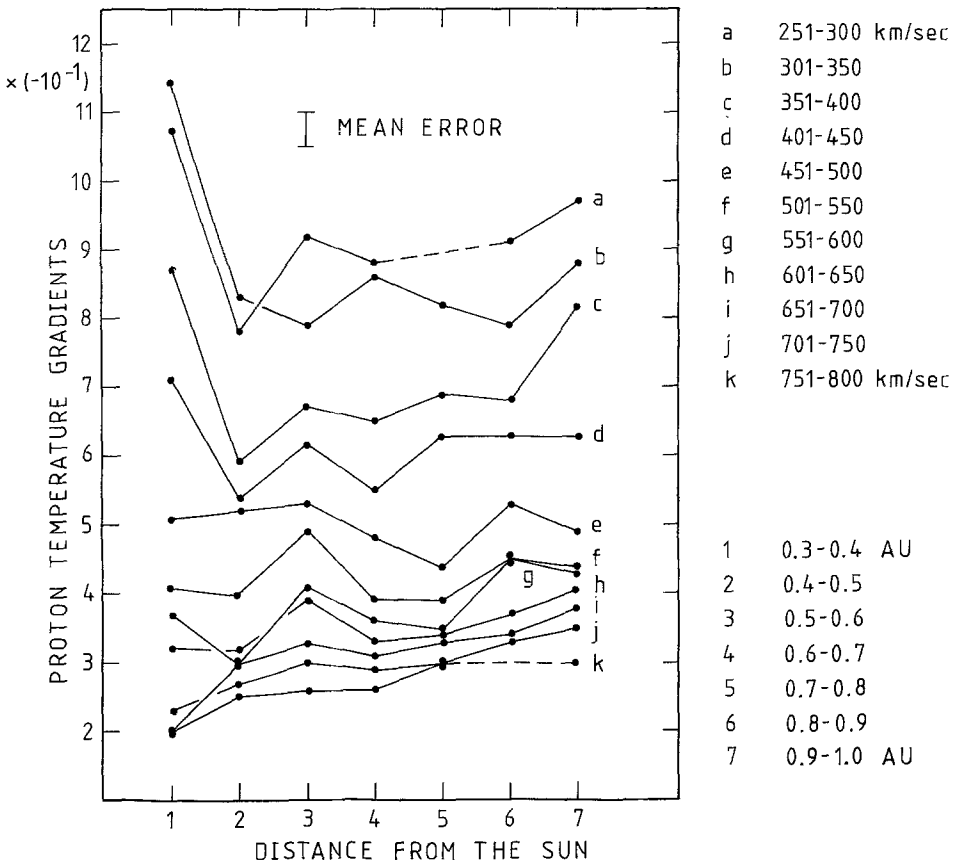

Fig. 10. The calculated proton temperature radial gradients as a function of heliocentric distance and solar wind speed.

this way, we determine an upper threshold of the proton temperature for different distances and different speeds involving the radial temperature gradients. After comparison of these thresholds with the measured temperatures we could decide for a VLT case or not.

For the calculation of the gradients, we devide the distance explored by Helios-1 (0.3–1.0 AU) into seven equal consequative parts (each 0.1 AU of width). The hourly plasma data measured by Helios-1 over the period December 1974–December 1977 are used (~16000). Because, as it is well known (Rosenbauer *et al.*, 1977), solar wind with different speeds behaves also differently, concerning the heat conduction processes, we calculate the temperature gradients also as a function of the solar wind speed. In these calculations, we do not remove data exhibiting interplanetary shock waves or tangential discontinuities or fast solar wind streams, involving different physical mechanisms than the normal wind. By averaging all solar wind structures, we intend to derive general radial temperature gradients for this long period. The solar wind speed is devided into eleven equal contiguous intervals in a total range of 250 to 800 km s^{-1},

TABLE II
Radial proton temperature gradients (b)

R (AU) V (km s^{-1})	0.3–0.4	0.4–0.5	0.5–0.6	0.6–0.7	0.7–0.8	0.8–0.9	0.9–1.0
250–300	1.07 ± 0.05	0.78 ± 0.08	0.92 ± 0.30	0.88 ± 0.08	—	0.91 ± 0.1	0.97 ± 0.2
301–350	1.14 ± 0.03	0.83 ± 0.04	0.79 ± 0.06	0.86 ± 0.05	0.82 ± 0.05	0.79 ± 0.04	0.88 ± 0.03
351–400	0.87 ± 0.03	0.59 ± 0.04	0.67 ± 0.04	0.65 ± 0.04	0.69 ± 0.03	0.68 ± 0.03	0.82 ± 0.02
401–450	0.71 ± 0.07	0.54 ± 0.04	0.62 ± 0.04	0.55 ± 0.04	0.63 ± 0.03	0.63 ± 0.03	0.63 ± 0.03
451–500	0.51 ± 0.04	0.52 ± 0.06	0.53 ± 0.03	0.48 ± 0.05	0.44 ± 0.03	0.53 ± 0.03	0.49 ± 0.02
501–550	0.41 ± 0.03	0.40 ± 0.05	0.49 ± 0.04	0.39 ± 0.04	0.39 ± 0.03	0.45 ± 0.03	0.44 ± 0.02
551–600	0.37 ± 0.03	0.30 ± 0.04	0.41 ± 0.03	0.36 ± 0.05	0.35 ± 0.03	0.45 ± 0.03	0.43 ± 0.02
601–650	0.32 ± 0.03	0.32 ± 0.03	0.39 ± 0.03	0.33 ± 0.05	0.34 ± 0.03	0.37 ± 0.04	0.41 ± 0.02
651–700	0.20 ± 0.04	0.30 ± 0.04	0.33 ± 0.03	0.31 ± 0.04	0.33 ± 0.04	0.34 ± 0.03	0.38 ± 0.03
701–750	0.23 ± 0.05	0.27 ± 0.05	0.30 ± 0.03	0.29 ± 0.03	0.30 ± 0.05	0.33 ± 0.05	0.35 ± 0.03
751–800	0.20 ± 0.06	0.25 ± 0.2	0.26 ± 0.06	0.26 ± 0.06	0.30 ± 0.1	—	0.30 ± 0.09

(each 50 km s^{-1} of width). For the calculations, we correlate the magnitude ln T/T_0 with the ln $R/R_\odot$ linearly; T, T_0 are the proton temperatures at distances R, $R_\odot$, respectively. (For normalization purposes, we substitute T_0 with 1.2×10^6 K and $R_\odot$ with $2R_\odot$; these values are simply taken from the Hartle and Barnes two-fluid model (1970).)

These temperature gradients are shown in Figure 10 as a function of distance and solar wind speed. The numerical values and their errors are in Table II. It is evident, from Figure 10, that on the average, the gradients are decreasing as the solar wind speed is increasing, (for example, the mean gradient at low speeds is by a factor of three larger than at high speeds). As the solar wind becomes slower, the corresponding gradients approach the value characterized an adiabatic expansion. From the same figure, it seems that for very slow solar wind the gradients are higher nearer to the Sun than away from it. For higher speeds, on the average, the gradients are constant in the range 0.3 to 1.0 AU. It seems, that for very fast solar wind, on the contrary, gradients are steeper as the distance from the Sun increases.

Using a different way of calculating proton temperature gradients, Schwenn *et al.* (1978), based on eight radial line-up constellations between Helios-1 and Helios-2, found for three intervals (slow, up to 400 km s^{-1}, intermediate and fast) the values -1.2 ± 0.1, -0.76 ± 0.11, and -0.69 ± 0.08, respectively.

4. The 'Closed' Models

Assuming that the 'cool' regions are due to a nearly magnetically closed structures, which are convected by the solar wind with a constant speed, expanding away from the Sun, we intend to estimate the distance of their origin, if these structures do exist in the solar wind.

For this estimation, we have to know how the temperature inside and outside this region varies with distance – i.e., two relations between distance and temperature, one

for inside the other for outside. The distance in which the temperature inside equals with this outside should be the formation distance of the closed regions. As input values of distance and temperature into these relations, we use the temperature measurements of Helios-1 and Helios-2 in different heliocentric distances.

This model is a modified version of a similar model treated by Geranios (1978), with two main differences. One, the expansion here is not assumed as being adiabatic (i.e., the polytropic index is not equal to $\frac{5}{3}$) and two, the temperature gradients of the ambient solar wind, needed for the temperature variation outside the cold regions, are calculated from the experimentally measured data of Helios-1.

For the temperature inside (thereafter as T_i), we use the equation

$$T_i = T_0(r/r_0)^{-2(\gamma-1)} \tag{1}$$

where T_i and T_0 are the temperatures at distances r and r_0; and γ is the polytropic index. The derivation of Equation (1) as well the basic models are analytically described in the previously mentioned paper by Geranios.

For the relation concerning the temperature variation in the ambient solar wind (outside the closed structure, thereafter as T_a), we use two different relations. One, valid for distances $2R_\odot$–$38R_\odot$, the other for distances $38R_\odot$–$214R_\odot$: i.e.,

$$T_a = T_0(r/r_0)^{-a} \quad \text{for} \quad 2R_\odot \leq r < 38R_\odot, \tag{2.1}$$

$$T_a = T_0(38/r_0)^{-a}(r/38)^{-b} \quad \text{for} \quad 38R_\odot \leq r < 214R_\odot, \tag{2.2}$$

when $a = 0.349$ (Hartle and Barnes, 1970); and b denotes the proton temperature gradient of the ambient solar wind.

With Equations (1), (2.1), and (2.2) we have

$$r_0 = r(T_i/T_a)^{1/[2(\gamma-1)-a]} \quad \text{for} \quad 2R_\odot \leq r < 38R_\odot, \tag{3.1}$$

$$r_0 = (T_i/T_a)^{1/[2(\gamma-1)-a]} \times 38^{(a-b)/[a-2(\gamma-1)]} \times \\ \times r^{[b-2(\gamma-1)]/[a-2(\gamma-1)]}, \tag{3.2}$$

valid for $38R_\odot \leq r < 214R_\odot$. T_i and T_a are measured for each of the cases listed in Table I (f. ex. in Figure 4, $T_i = 2 \times 10^4$ K, $T_a = 6 \times 10^4$ K and 8×10^4 K); r_0 is the formation heliocentric distance of the closed structures.

If we assume in the same model that the rate of pressure equalization across the boundary of the structure is assumed to be much greater than the rate of the expansion ($1/\tau_p \gg 1/\tau$), we obtain an analogous equation (1) (cf. Geranios, 1978)

$$T_i = T_0(r/r_0)^{-(\gamma-1)(\varepsilon+2)/\gamma}, \tag{4}$$

and $\varepsilon = 0.316$ is the temperature gradient for electrons, suggested by the Hartle and Barnes two-fluid solar wind model (1970).

With Equation (2.1) and (2.2), Equation (4) becomes

$$r_0 = r(T_i/T_a)^{1/[[(\gamma-1)(\varepsilon+2)/\gamma]-a]} \quad \text{for} \quad 2R_\odot \leq r < 38R_\odot, \tag{4.1}$$

$$r_0 = (T_i/T_a)^{1/[[(\gamma-1)(\varepsilon+2)/\gamma]-a]} \times 38^{-(a-b)/[[(\gamma-1)(\varepsilon+2)/\gamma]-a]} \times$$
$$\times\, r^{[b-(\gamma-1)(\varepsilon+2)/\gamma]/[a-(\gamma-1)(\varepsilon+2)/\gamma]} \quad \text{for} \quad 38R_\odot \leq r < 214R_\odot, \tag{4.2}$$

T_i and T_a are the same measured temperatures as before; r_0 is the formation distance of the closed structures, according to the second version of the model.

The model characterized by Equations (1), (3.1), and (3.2) is named thereafter as model I. The model characterized by Equations (4), (4.1), and (4.2) is model II.

5. Calculation of the Polytropic Indeces

The magnetically closed structure is assumed here as not being completely thermally isolated from the ambient solar wind, which means that the polytropic index should be not equal to $\frac{5}{3}$, which characterizes an adiabatic expansion (as in a fully ionized gas with three degrees of freedom; cf. Spitzer (1962)).

Therefore, we calculate from experimentally also derived data new polytropic indeces for the two models.

For model I we use Equation (1), for model II we use Equation (4). For the estimation of T_0 and r_0 we use the boundary conditions of the H-B model – i.e.,

$$T_0 = 1.2 \times 10^6\,\mathrm{K} \quad \text{at} \quad r_0 = 2R_\odot.$$

For the values of T and r, we apply the proton low temperatures measured at the corresponding heliocentric distances as listed in Table I, (T_m).

5.1. Model I

Equation (1) gives

$$\ln(T_i/T_0) = A \ln(r/r_0), \tag{5}$$

where $A = -2(\gamma_\mathrm{I} - 1)$; index I applying to model I.

The least-squares method applied to Equation (5) between $\ln(T_i/T_0)$ and $\ln(r/r_0)$ determines A and therefore

$$\gamma_\mathrm{I} = 1.49 \pm 0.03.$$

5.2. Model II

Equation (4) gives

$$\ln(T_i/T_0) = B \ln(r/r_0), \tag{6}$$

where $B = -(\gamma_\mathrm{II} - 1)(\varepsilon + 2)/\gamma_\mathrm{II}$, II applies to model II.

With the same method applied to model I, we estimate B and, therefore,

$$\gamma_\mathrm{II} = 1.73 \pm 0.07.$$

6. Test of the Models

Because our measurements are restricted within a distance between 65 and $214R_\odot$ (0.3 and 1.0 AU), we apply Equation (3.2) for model I and Equation (4.2) for model II. Substitution of one pair of T_i, r, ($T_i = T_m$) into these equations, gives one distance r_0. Since the outside temperatures of the closed region (which also define the 'width' of the region) are two (T_1, T_2 in Table I), we calculate two also values of r_0 indicating the range, in which the structure is formed. On the other hand, the value of the exponent b, representing the proton radial gradients, is not the same for all cases presented in Table I, but it depends, as it was mentioned, on the heliocentric distance and on the solar wind speed. As it is shown in Table II, b can have 75 values. After the distinction between γ's and the variability of b, Equations (3.2) and (4.2) are

$$r_{0,i} = (T_i/T_a)^{1/[2(\gamma_I - 1) - a]} \times 38^{(a - b_i)/[a - 2(\gamma_I - 1)]} \times \\ \times r^{[b_i - 2(\gamma_I - 1)]/[a - 2(\gamma_I - 1)]} \quad \text{for model I,} \tag{7.1}$$

$$r_{0,i} = (T_i/T_a)^{1/[[(\gamma_{II} - 1)(\varepsilon + 2)/\gamma_{II}] - a]} \times 38^{-(a - b_i)/[[\gamma_{II} - 1)(\varepsilon + 2)/\gamma_{II}] - a]} \times \\ \times r^{[b_i - (\gamma_{II} - 1)(\varepsilon + 2)/\gamma_{II}]/[a - (\gamma_{II} - 1)(\varepsilon + 2)/\gamma_{II}]} \quad \text{for model II;} \tag{7.2}$$

both equations for $38R_\odot \leq r < 214R_\odot$. Subscript i indicates the 75 different values of b; r is the radial distance of the observation.

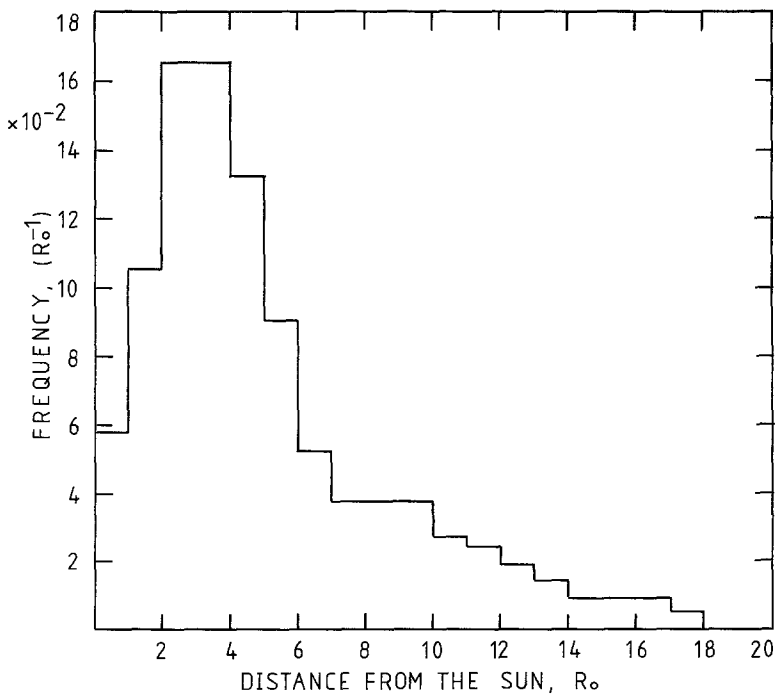

Fig. 11. The frequency distribution of the formation distance of the VLT's.

TABLE III
The calculated Ranges (Ro) of the origin of the 'closed' structures

No.	Model I Range	Model II Range	No.	Model I Range	Model II Range	No.	Model I Range	Model II Range
1	5.7–12.7	5.6–12.6	30	2.0–5.5	2.0–5.4	59	4.2–4.9	4.1–4.8
2	10.7–16.8	10.5–16.6	31	0.8–1.6	0.8–1.6	60	4.6–5.9	4.5–5.8
3	0.4–0.8	0.4–0.8	32	1.3–1.4	1.2–1.3	61	1.3–5.1	1.3–5.1
4	0.9–5.0	0.9–4.9	33	0.4–3.9	0.4–3.8	62	2.5–2.9	2.5–2.9
5	0.2–1.7	0.2–1.7	34	2.0–2.1	2.0–2.1	63	2.2–3.9	2.2–3.8
6	2.9–3.2	2.9–3.1	35	2.6–3.0	2.5–2.9	64	0.2–4.0	0.2–3.9
7	1.8–5.3	1.7–5.2	36	3.2–3.7	3.2–3.7	65	3.8–4.4	3.7–4.3
8	3.2–3.4	3.2–3.4	37	2.5–2.9	2.4–2.8	66	0–0.2	0–0.2
9	6.5–7.1	6.4–7.0	38	4.9–5.8	4.9–5.7	67	1.4–1.5	1.3–1.5
10	2.9–3.4	2.8–3.3	39	2.1–4.7	2.0–4.6	68	2.9–3.4	2.9–3.4
11	1.5–2.8	1.5–2.8	40	1.1–5.6	1.0–5.5	69	2.5–2.9	2.5–2.9
12	5.5–14.2	5.4–14.1	41	0.8–3.7	0.8–3.6	70	0.6–5.1	0.6–5.1
13	0.4–3.4	0.4–3.3	42	6.8–12.9	6.7–12.7	71	2.4–7.2	2.4–7.1
14	4.8–5.6	4.7–5.5	43	2.3–5.1	2.2–5.0	72	1.9–2.6	1.8–2.5
15	0.6–1.3	0.6–1.3	44	0.3–2.2	0.3–2.2	73	4.2–4.3	4.1–4.3
16	1.0–4.7	1.0–4.7	45	3.4–3.9	3.3–3.9	74	5.0–9.5	4.9–9.3
17	0.4–1.3	0.4–1.3	46	2.0–6.0	2.0–5.9	75	1.5–3.4	1.5–3.4
18	0.2–1.1	0.2–1.0	47	2.6–3.7	2.6–3.7	76	2.4–5.4	2.4–5.3
19	0.9–6.0	0.9–5.9	48	3.8–4.5	3.8–4.4	77	0.7–4.1	0.7–4.0
20	1.7–1.9	1.6–1.9	49	1.0–6.7	1.0–6.6	78	2.7–4.1	2.7–4.0
21	1.1–3.2	1.0–3.1	50	3.1–4.8	3.0–4.8	79	2.9–3.4	2.9–3.4
22	0.8–5.6	0.8–5.5	51	2.0–6.1	2.0–6.0	80	1.9–2.9	1.8–2.9
23	1.6–11.1	1.6–11	52	4.1–5.0	4.0–4.9	81	1.9–6.3	1.8–6.2
24	2.3–3.2	2.2–3.2	53	2.2–4.1	2.1–4.0	82	1.5–4.4	1.4–4.3
25	0.3–7.1	0.3–7.0	54	3.2–16.9	3.1–16.7	83	2.0–2.6	1.9–2.6
26	0.3–1.6	0.3–1.6	55	2.6–11	2.5–10.9	84	4.4–5.1	4.4–5.0
27	1.3–1.5	1.3–1.4	56	0.3–1.0	0.3–1.0	85	1.1–1.3	1.1–1.3
28	2.1–2.2	2.0–2.2	57	0.5–2.4	0.5–2.4	86	2.5–2.9	2.5–2.9
29	1.2–1.3	1.2–1.3	58	1.5–10.3	1.5–10.2	87	3.9–4.6	3.8–4.5

For all cases listed in Table I the calculated ranges of r_0 are shown in Table III.

For the speed classification, we considered the mean speed ($V_{\text{mean}} = [V_m + V_1 + V_2]/3$). The corresponding histogram representing the frequency distribution of the distances in which the closed structures may be originated is shown in Figure 11. Because for both models the calculated ranges are almost the same (Table III), we have plotted one frequency distribution only. The total range of the distance is $18R_\odot$. The highest frequency near 2 to $4R_\odot$ places the origin of the structures very close to the Sun.

7. Discussion

In the previously tested models, the determined mean distance of the formation of the examined structures, does not much differ from the distance derived from measurements at 1 AU (Geranios, 1979). In that treatment, for model II, this distance for protons is found between 2 and $10R_\odot$. Because in the present analysis, electron

temperature data were not available, we could not be able to calculate an analogous distribution for electrons too.

The fact that a considerable large number of listed VLT's (Table I) are coincident with a sector boundary passage (example of Figure 8), supports the closed structure model, since in the boundaries we have opposite directed interplanetary magnetic fields, favorable for such structures. Marsch *et al.* (1978), based on Helios data, observed also dips in the profiles of temperature and heat flux associated with magnetic sector boundaries. Especially, the association of reduced heat flux with sector boundaries suggests a thermically isolated, from the ambient solar wind, closed structure model.

An other example, for the correlation between low proton temperatures and magnetic sector boundaries, is reported by Borini *et al.* (1980), on a verification of signals of coronal streamers in the solar wind at 1 AU. Based on IMP-6, 7, and 8 data during 1971–1978, they reported that the superimposed epoch analysis of 74 well defined sector boundary crossings correlates, among others, with low kinetic temperatures of solar wind protons.

An other couple of examples of similar structures, not necessarily associated with sector boundaries, are reported by Krimigis *et al.* (1976), and recently, by Bame *et al.* (1980). The former, by anisotropy observations of protons with energies $0.29 < E_p < 0.5$ MeV and electrons with energies $E_e > 0.22$ MeV; in most cases there were sunward flows which were preceded or followed by sustained anti-sunward flows suggesting a closed loop-like structure in the interplanetary magnetic field. The latter, by bi-directional streaming observation of solar electrons with energies $E_e > 100$ eV. This observation, based on ISEE-3 data in the interplanetary space, was related with a large solar flare on 10 November, 1978. The streaming was aligned with the interplanetary magnetic field which was roughly perpendicular to the Sun-satellite line. They also found similar bi-directional streaming near the bow shock when field connection to the shock allows an upstream flow of heat from the shock to coexist with the outward flow of heat from the Sun. Concluding, they suggest that this event is best explained by an interplanetary field geometry similar either to a magnetic bottle rooted at the Sun or to a disconnected loop propagating outward. This second possibility coincides with our model. Even if one could assume that the electron streaming toward the Sun is due to a reflection of the bow shock and not to a closed magnetic field, then, this phenomenon should not be present at distances far from the bow shock. On the contrary, we have found a plenty of such structures very far from the shock, (Helios-observations).

The pi-like features shown in Figures 4, 5, and 6, are characterized with simultaneous enhancements and dips of the IMF magnitude and azimuth, during which the proton temperature remaines at depressed values. In Figure 4, the direction of the field (ϕ) displays smaller variations at 06 and 14 UT than the direction of the field in Figure 6 at 04 and 12 UT. For a possible explanation of this observation, we propose a very schematical picture projected onto the ecliptic plane, showing within a magnetic sector the passage of two successive closed structures (Figure 12). The structures are assumed to be ideal spheres propagating away from the Sun. The satellite observes, as these structures pass away, alternate magnetic field directions. If the passage is central (in Figure 12

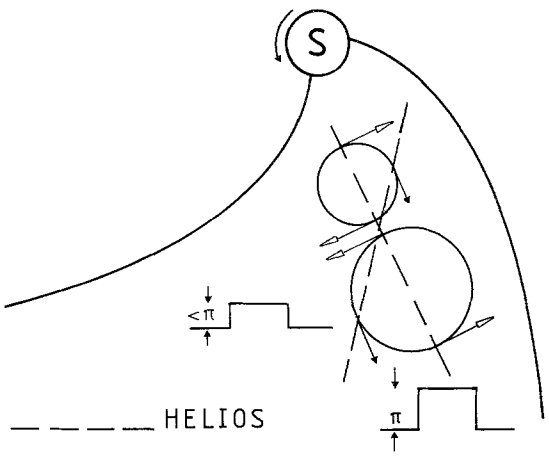

Fig. 12. The projection onto the ecliptic plane of two 'closed' structures, moving radially from the Sun within a magnetic sector (very schematical). Dashed lines, indicate the interacts between the structures and the observing satellite. If the passage is central, a 180° variation of the angle ϕ is expected, if not, this variation is less. In both cases, because of the same direction of the magnetic field between the structures, B is expected to increase.

shown as a nearly radial direction), the variation of ϕ should be maximum, ($\Delta\phi = \pi$). If the passage is not central (shown as a tilted direction), the variation of ϕ should be less ($\Delta\phi < \pi$). Nevertheless, in both cases, between the two structures the magnetic field magnitude should be enhanced, (because of the similar direction of ϕ). This last point can be also visualized in the examples of Figures 4 and 6, by the simultaneous enhancement of the field (B).

8. Conclusions

From the treatment of the models, it came out that whether the test is made with measurements at constant heliocentric distances (1 AU), or not (0.3–1.0 AU), the average distance of the formation of the closed structures is the same.

A very important point, which one should emphasize in the whole treatment of the phenomenon, is the fact that a very low temperature is an effect which arises from the interplanetary medium between the solar corona and the observational point, and not from a cold plasma ejection from the Sun. In other words, we assume that the VLT's are observed not because the corona was localy cold, but because in the solar wind steeper temperature gradients were present (for example, because of the closed structures). To distinguish one from the other possibilities, one should compare the calculated temperature gradient at the magnetic sector boundaries with the gradient within magnetic sectors. If the first is systematically steeper from the second, then, the solar wind origin and not the coronal origin should be the more probable.

More numerous events of VLT's observed by Helios-1 and Helios-2 are needed for the interpretation of this phenomenon, especially, an increase of such observations

closer to the Sun could support the closed structure models, as generally, at very far distances magnetically closed structures are considered as rare.

Acknowledgments

We express our gratitudes to S. J. Bame for the supported plasma data at 1 AU (IMP), H. Rosenbauer and F. Neubauer for the Helios-1 and Helios-2 interplanetary plasma and magnetic field data, respectively.

References

Bame, S., Asbridge, J., Feldman, W. and Gosling, J.: 1976, *Astrophys. J.* **207,** 977.
Bame, S., Asbridge, J., Feldman, W., Gosling, J. and Zwickl, R.: 1980, *Trans. AGU* **61,** 1096.
Borini, G., Gosling, J., Bame, S., Feldman, W. and Wilcox, J.: 1980, *Trans. AGU* **61,** 1097.
Chamberlain, J.: 1965, *Astrophys. J.* **141,** 320.
Durney, B.: 1971, *Astrophys. J.* **166,** 669.
Feldman, W., Asbridge, J., Bame, S. and Montgomery, M.: 1973, *J. Geophys. Res.* **78,** 6451.
Geranios, A.: 1978, *Planetary Space Sci.* **26,** 571.
Geranios, A.: 1979, *Proc. Int. Conf. Cosmic Rays, Kyoto* **3,** 134.
Geranios, A.: 1980, *Nuovo Cimento* **3C,** 382.
Geranios, A.: 1981, *Astrophys. Space Sci.* **77,** 167.
Gosling, J. and Roelof, E.: 1974, *Solar Phys.* **39,** 405.
Gosling, J., Pizzo, V. and Bame, S.: 1973, *J. Geophys. Res.* **78,** 2001.
Hartle, R. and Barnes, A.: 1970, *J. Geophys. Res.* **75,** 6915.
Hundhausen, A.: 1972, *Coronal Expansion and Solar Wind*, Springer, Berlin, Heidelberg, New York.
Krimigis, S., Sarris, E. and Armstrong, T.: 1976, *Trans. AGU* **57,** 304.
Marsch, E., Pilipp, W., Schwenn, R., Mühlhäuser, K. and Rosenbauer, R.: 1978, *Proc. Int. Conf. Solar Wind*, Burghausen, F.R.G.
Montgomery, M., Bame, S. and Hundhausen, A.: 1968, *J. Geophys. Res.* **73,** 4999.
Montgomery, M., Asbridge, J., Bame, S. and Feldman, W.: 1974, *J. Geophys. Res.* **79,** 3103.
Neubauer, F., Beinroth, H., Barnstorf, H. and Dehmel, G.: 1977, *J. Geophys.* **42,** 599.
Noble, L. and Scarf, F.: 1963, *Astrophys. J.* **138,** 1169.
Parker, E.: 1958, *Astrophys. J.* **128,** 664.
Parker, E.: 1964, *Astrophys. J.* **139,** 93.
Parker, E.: 1965, *Space Sci. Rev.* **4,** 666.
Rosenbauer, H., Schwenn, R., Marsch, E., Meyer, B., Miggenrieder, H., Montgomery, M., Mühlhäuser, K., Pilipp. W. and Zink, S.: 1977, *J. Geophys.* **42,** 561.
Schwenn, R., Mühlhäuser, K., Marsch, E. and Rosenbauer, H.: 1978, *Proc. Int. Conf. Solar Wind*, Burghausen, F.R.G.
Spitzer, L.: 1962, *Physics of Fully Ionized Gases*, Interscience, New York.
Sturrock, P. and Hartle, R.: 1966, *Phys. Rev. Letters* **10.** 631.
Whang, Y. and Chang, C.: 1965, *J. Geophys. Res.* **70,** 4175.
Yeh, T.: 1970, *Planetary Space Sci.* **18,** 1999.